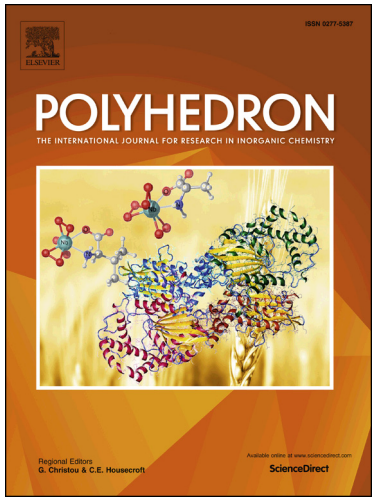

Transition metal chelate complexes with tetrazole derived Mannich base: metal dependent architecture and properties

Inna M. Grigorieva, Tatiyana V. Serebryanskaya, Yuri V. Grigoriev, Alexander S. Lyakhov, Ludmila S. Ivashkevich, Artem S. Bogomyakov, Ludmila G. Lavrenova, Sergei V. Voitekhovich, Oleg A. Ivashkevich

PII: S0277-5387(18)30250-X
DOI: https://doi.org/10.1016/j.poly.2018.05.012
Reference: POLY 13159

To appear in: *Polyhedron*

Received Date: 25 March 2018
Accepted Date: 6 May 2018

Please cite this article as: I.M. Grigorieva, T.V. Serebryanskaya, Y.V. Grigoriev, A.S. Lyakhov, L.S. Ivashkevich, A.S. Bogomyakov, L.G. Lavrenova, S.V. Voitekhovich, O.A. Ivashkevich, Transition metal chelate complexes with tetrazole derived Mannich base: metal dependent architecture and properties, *Polyhedron* (2018), doi: https://doi.org/10.1016/j.poly.2018.05.012

Transition metal chelate complexes with tetrazole derived Mannich base: metal dependent architecture and properties

Inna M. Grigorieva,[a] Tatiyana V. Serebryanskaya,[a] Yuri V. Grigoriev,[a] Alexander S. Lyakhov,[a] Ludmila S. Ivashkevich,[a] Artem S. Bogomyakov,[b] Ludmila G. Lavrenova,[c] Sergei V. Voitekhovich,*[a] Oleg A. Ivashkevich[d]

[a]*Research Institute for Physical Chemical Problems of Belarusian State University, Leningradskaya 14, 220006 Minsk, Belarus*

[b]*International Tomography Center, Siberian Branch of the Russian Academy of Sciences, Institutskaya 3a, 630090 Novosibirsk, Russia*

[c]*Nikolaev Institute of Inorganic Chemistry, Siberian Branch of the Russian Academy of Sciences, Acad. Lavrentiev avenue 3, 630090 Novosibirsk, Russia*

[d]*Belarusian State University, Nezalezhnasti avenue 4, 220050 Minsk, Belarus*

Abstract

Complexes $[Cu_2L_2Cl_4]$, $[NiL_2Cl_2]$, $[PdLCl_2]$, and $[PtLCl_2]$, where L is a novel ligand from the series of 2-subsituted 5-(α-aminoalkyl)tetrazoles, namely 5-(*N*,*N*-dimethylaminomethyl)-2-*tert*-butyltetrazole, have been synthesized and characterized by IR spectroscopy, thermal analysis and single crystal X-ray analysis. The complexes reported show different coordination geometries of the metals, *viz.* octahedral for Ni, square pyramidal for Cu, and square planar for Pt and Pd complexes. At the same time, the ligand L demonstrates the same coordination mode in all the complexes. It acts as a chelating ligand coordinated to the metal *via* two nitrogen atoms, namely the tetrazole ring N^4 and the dimethylamino N atoms. Complex $[PtLCl_2]$ was found to have promising antiproliferative activity against human cervical carcinoma cells, with IC_{50} value being average between those of cisplatin and carboplatin. The temperature-dependent magnetic susceptibility measurements of complex $[Cu_2L_2Cl_4]$ revealed that the copper(II) ions were weakly antiferromagnetically coupled showing a coupling constant *J* of -2 cm^{-1}.

Keywords: Metallocomplexes; Tetrazoles; Cytotoxicity; Magnetic properties

1. Introduction

Mannich bases of CH- and NH-acidic azoles (HetH) with general formula Het-CH_2NR_2 are of interest due to their wide range of bioactivity [1,2]. Introduction of the aminomethyl group as a side chain to azoles is used to increase their aqueous solubility and thereby to improve the bioavailability, that is important for drug design. Moreover, the presence of several donor heteroatoms in azole rings and additional amino group in α-position of the side chain makes the above compounds attractive as multidentate ligands, providing diverse coordination modes including chelating ones. Although direct C- and N-aminomethylation was previously reported for parent tetrazole and its 1- and 5-monosubstituted derivatives [3,4], very little has appeared in the literature concerning the coordination chemistry of corresponding Mannich bases. Only the preparation and structure of copper(II) complexes with *N*,*N*-dimethyl-1-(1-methyl-1*H*-tetrazol-5-yl)methanamine [5] and 5-aminomethyl-1*H*-tetrazole [6] have been published.

Herein, we report the preparation, thermal behavior and single crystal X-ray analysis of copper(II), nickel(II), platinum(II) and palladium(II) chloride complexes with a Mannich base, namely 5-(*N*,*N*-dimethylaminomethyl)-2-*tert*-butyltetrazole (**1**). Additionally, magnetic properties of the synthesized copper(II) complex and antiproliferative activity of the platinum(II) complex have been also investigated.

2. Experimental section

2.1. Materials and instrumentation

All reagents and solvents were obtained from commercial sources and used without purification. Elemental analyses for C, H, and N were performed on a FlashEA 1112 analyzer. ^{1}H and ^{13}C NMR spectra were recorded on a Bruker Avance 500 spectrometer at 500 and 125 MHz, correspondingly. The observed chemical shifts were referenced to the solvent signals (DMSO-d_6, δ_H 2.50, δ_C 39.43). FT-IR absorption spectra were recorded in the range 4000–400 cm^{-1} on a Thermo Nicolet Avatar 360 spectrometer. The TG and DSC curves were obtained using a NETZSCH STA429 thermoanalyzer in a dynamic nitrogen atmosphere (heating rate 10 °C min^{-1}, aluminium oxide, mass 1–3 mg, temperature range from room temperature to 500 °C). The magnetic susceptibility of copper(II) complex was measured on a polycrystalline sample using a Quantum Design MPMS*XL* SQUID magnetometer in the temperature range 5–300 K with magnetic field of up to 5 kOe. Diamagnetic corrections were made using the Pascal constants. The effective magnetic moment was calculated as $\mu_{eff}(T) = [(3k/N_A\mu_B^2)\chi T]^{1/2} \approx (8\chi T)^{1/2}$.

2.2. Synthesis of the compounds

*2.2.1. Synthesis of 5-(N,N-dimethylaminomethyl)-1H-tetrazole (**2**)*

Compound **2** was synthesized following a procedure described in the literature [3]. A mixture of 1*H*-tetrazole (10.5 g, 150 mmol), dimethylamine hydrochloride (12.23 g, 150 mmol), paraformaldehyde (6.9 g, 230 mmol), 5–6 drops of concentrated hydrochloric acid, benzene (75 mL), and nitrobenzene (75 mL) was heated to reflux in Dean-Stark apparatus for 4 h. Then the reaction mixture was cooled to room temperature and the solvent was decanted. 2-Propanol (250 mL) and solution of sodium hydroxide (6 g, 150 mmol) in water (45 mL) were added to the residue. The mixture obtained was boiled for 10 min, then filtered while hot, cooled to −15 °C and held at this temperature for 2 days. Brownish crystals of **2** (Yield 9.86 g, 52 %) were isolated by filtration of the above cold mixture. ^{1}H NMR δ (ppm): 4.28 (s, 2H, CH_2), 2.63 (s, 6H, 2Me); ^{13}C NMR δ (ppm): 153.1 (CN_4), 51.3 (CH_2), 42.6 (2Me). *Anal.* Calcd for $C_4H_9N_5$: C, 37.79; H, 7.13; N, 55.08. Found: C, 37.66; H, 7.20; N, 54.85.

*2.2.2. Synthesis of 5-(N,N-dimethylaminomethyl)-2-tert-butyltetrazole (**1**)*

tert-Butyl alcohol (0.70 g, 9.4 mmol) was added dropwise with stirring to a solution of **2** (1.07 g, 8.5 mmol) in conc. sulfuric acid (6 mL). Then the reaction mixture was kept at room temperature for 1 h, poured into 35 g of ice-water mixture, neutralized with aqueous sodium hydroxide (25 %, 30 mL), and extracted with benzene (3×20 mL). The combined extract was dried over anhydrous potassium carbonate, and evaporated to give **1** as yellowish oil (Yield 80 %, 1.20 g). *Anal.* Calcd for $C_8H_{17}N_5$: C, 52.43; H, 9.35; N, 38.22. Found: C, 52.60; H, 9.50; N, 37.95. ^{1}H NMR δ (ppm): 3.68 (s, 2H, CH_2), 2.13 (s, 6H, 2Me), 1.67 (s, 9H, 3Me); ^{13}C NMR δ (ppm): 162.3 (CN_4), 63.2 (C), 52.5 (CH_2), 44.4 (2Me), 28.6 (3Me). FT-IR (cm^{-1}): 2983 s, 2941 s, 2865 s, 2823 s, 2774 s, 1497 m, 1461 s, 1400 m, 1732 s, 1348 m, 1311 s, 1263 m, 1235 m, 1197 s, 1171 s, 1143 m, 1099 w, 1074 w, 1030 s, 852 m, 828 m, 804 m, 715 m, 703 m, 591 m, 505 w, 497 w.

*2.2.3. Synthesis of $[Cu_2L_2Cl_4]$ (**3**) and $[Cu_2L_2Cl_4]\cdot 2CHCl_3$ (**3s**)*

$CuCl_2\cdot 2H_2O$ (106 mg, 0.62 mmol) was added to a solution of **1** (110 mg, 0.62 mmol) in 1,2-dichloroethane (20 mL). The resulting mixture was stirred at room temperature for 6 h and filtered to remove unreacted salt. Slow evaporation of the obtained solution at ambient conditions gave green crystals of complex **3** (Yield 75 %, 147 mg). *Anal.* Calcd for $C_{16}H_{34}Cl_4Cu_2N_{10}$: C, 30.24; H, 5.39; N, 22.04. Found: C, 30.45; H, 5.18; N, 21.85. FT-IR (cm^{-1}): 3020 m, 2983 s, 2935 s, 2915 s, 2794 w, 1520 m, 1462 s, 1403 m, 1374 s, 1340 m, 1307 s, 1277 m, 1284 m, 1203 s, 1180 s, 1111 m, 1073 w, 1028 s, 995 s, 941 w, 831 s, 809 s, 781 m, 712 m,

594 m, 585 m 478 w, 403 w. Recrystallization of **3** from chloroform–toluene mixture gave green crystals of solvated complex $[Cu_2L_2Cl_4]\cdot 2CHCl_3$, hereinafter referred to as complex **3*s***.

*2.2.4. Synthesis of [NiL$_2$Cl$_2$] (**4**)*

$NiCl_2\cdot 6H_2O$ (74 mg, 0.31 mmol) was added to a solution of **1** (110 mg, 0.62 mmol) in 1,2-dichloroethane (20 mL). The resulting mixture was stirred at room temperature for 18 h and filtered to remove unreacted salt. Slow evaporation of the obtained solution at ambient conditions gave green crystals of complex **4** (Yield 46 %, 71 mg). *Anal.* Calcd for $C_{16}H_{34}Cl_2N_{10}Ni$: C, 38.74; H, 6.91; N, 28.23. Found: C, 38.95; H, 7.02; N, 27.98. FT-IR (cm^{-1}): 2984 s, 2922 m, 2884 m, 1530 s, 1469 s, 1445 s, 1380 s, 1350 s, 1313 s, 1274 w, 1242 w, 1224 m, 1189 s, 1162 w, 1118 w, 1030 s, 1005 s, 977 m, 859 s, 830 w, 789 w, 712 w, 609 w, 538 w, 485 m, 409 w.

*2.2.5. Synthesis of [PdLCl$_2$] (**5**)*

$PdCl_2\cdot 2H_2O$ (107 mg, 0.5 mmol) was dissolved in 1M HCl aqueous solution (10 mL) under stirring at 50 °C. To the resulting solution, a solution of **1** (92 mg, 0.5 mmol) in ethanol (5 mL) was added under stirring, and the reaction mixture was cooled to room temperature. The precipitate formed was filtered off and recrystallized from hot acetonitrile to give orange crystals of complex **5** (Yield 78 %, 141 mg). *Anal.* Calcd for $C_8H_{17}Cl_2N_5Pd$: C, 26.65; H, 4.75; N, 19.42. Found: C, 26.80; H, 4.80; N, 19.22. FT-IR (cm^{-1}): 1533 m, 1466 s, 1432 m, 1406 w, 1310 m, 1268 w, 1238 m, 1203 m, 1180 vs, 333 s br.

*2.2.6. Synthesis of [PtLCl$_2$] (**6**)*

A solution of **1** (62 mg, 0.34 mmol) in ethanol (5 mL) was added to a solution of K_2PtCl_4 (140 mg, 0.34 mmol) in distilled water (5 mL) under stirring. The resulting mixture was stirred at room temperature for 6 h. The precipitate formed was filtered off and recrystallized from acetonitrile to give yellow crystals of complex **6** (Yield 75 %, 114 mg). *Anal.* Calcd for $C_8H_{17}Cl_2N_5Pt$: C, 21.39; H, 3.81; N, 15.59. Found: C, 21.20; H, 3.90; N, 15.44. FT-IR (cm^{-1}): 2988 s, 2938 s, 2885 w, 1537 m, 1464 s, 1406 w, 1373 s, 1346 сл, 1310 s, 1271 w, 1235 m, 1205 m, 1179 s, 1147 w, 1111 w, 1021 m, 949 m, 852 s, 823 m, 786 w, 696 w, 601 m, 550 m, 517 w, 457 w, 412 w, 333 w.

*2.3. X-ray structure determinations of complexes **3**, **3s** and **4–6***

Suitable single crystals of synthesized complexes were directly picked up from the reaction mixture. Single crystal X-ray data were collected on a SMART Apex II diffractometer using graphite monochromated Mo-K radiation (= 0.71073 Å) at a temperature of 100 K. The structures were solved by direct methods (SIR2014) [7] and refined on F^2 by the full-matrix least squares technique (SHELXL 2014) [8]. The intensities were corrected for absorption. Non-

hydrogen atoms were refined anisotropically. The hydrogen atoms were placed in calculated positions and refined in a "riding" model, with $U_{iso}(H) = 1.5U_{eq}(C)$ for the methyl groups and $U_{iso}(H) = 1.2U_{eq}(C)$ for the methylene groups. Molecular graphics was performed with the programs ORTEP-3 for Windows [9] and PLATON [10]. X-ray powder diffraction data of polycrystalline complexes **3–6** were used to control their purity. The powder patterns were recorded with an EMPYREAN diffractometer (PANalytical, Netherlands) using Cu-Ka radiation (Ni-filter) at room temperature (Figures S7–S11).

*2.4. Antiproliferative activity assay of complex **6***

Antiproliferative activity of platinum(II) complex [$PtLCl_2$] was measured against HeLa cell line using trypan-blue exclusion assay as described earlier [11]. Briefly, HeLa cells (human cervical carcinoma) were cultured as a monolayer in culture flasks covered with 199 medium (RIEM) supplemented with 10 % fetal calf serum (RIEM) and 100 lg/mL kanamycin. Stock 10^{-2} M solutions of tested compound was freshly prepared in dimethylsulfoxide (DMSO), and then dilutions in distilled water from 10^{-4} to 10^{-6} M were made. On the day of the experiment, 50, 100 or 200 μL of drug dilutions were added into the flasks with cell monolayer at final concentrations of 0–100 μM. The cells were incubated at 37.0 °C for 48 h. Then treated and control cell monolayers were versenized, and viable cells were counted using trypan-blue exclusion on a haemocytometer [12]. IC_{50} values (drug concentration required to inhibit 50% of cell growth) were calculated from three independent experiments using regression analysis of the data received.

3. Results and discussion

3.1. Synthesis

5-(*N*,*N*-Dimethylaminomethyl)-2-*tert*-butyltetrazole (**1**) was obtained by two-step synthesis from parent 1*H*-tetrazole (Scheme 1). At the first stage, *C*-aminomethylation of 1*H*-tetrazole was performed by action of dimethylamine hydrochloride and paraformaldehyde under reflux in benzene–nitrobenzene solution [3]. In this way 5-(*N*,*N*-dimethylaminomethyl)-1*H*-tetrazole (**2**) was obtained in 52 % yield. Subsequent alkylation of **2** was carried out by the action of *tert*-butyl alcohol in concentrated sulfuric acid giving tetrazole **1** in 80% yield.

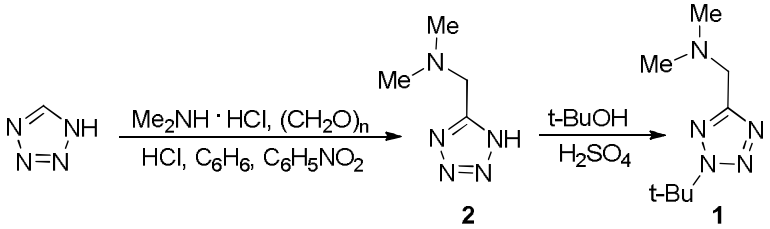

Scheme 1. Synthesis of target ligand **1**.

Acidic approach [13] was chosen for the alkylation in connection with recent success in adjusting the regioselectivity of *N*-functionalization of azoles using such approach [14–18]. In particular, it presents an efficient tool for introducing the lipophilic *tert*-butyl group into the N^2 position of the tetrazole cycle [13, 18]. The regioselectivity of alkylation of 5-R-tetrazoles is explained by the protonation of the tetrazole ring at the N^4 atom, resulting in the formation of 5-R-1*H*-4*H*-tetrazolium cations, in which only equivalent N^2 and N^3 atoms are accessible for attack by carbenium cations generated from the alkylation agents, like olefins and alcohols [13, 19]. The interaction of two positively charged entities seems rather unusual at first sight, however, quantum chemical calculations for a series of the above tetrazolium cations revealed that they show substantial electron density localized on N^2 and N^3 atoms [20]. The same mechanism is proposed for *tert*-butylation of **1** (Scheme 2). In this case, however, primary protonation at the amino N atom should be taken into account as well. Therefore, cation **A** acts as an alkylation substrate in highly acidic medium, such as sulfuric acid. Interaction of **A** with the *tert*-butyl cation, generated from the alcohol, leads to dication **B**. The latter undergoes deprotonation under alkaline work-up of reaction mixture forming 2,5-disubstituted tetrazole **1**. The obtained compound **1** was identified based on ^1H and ^{13}C NMR data. In particular, ^{13}C NMR chemical shift of the tetrazole ring C^5 atom of 162.3 ppm is in accordance with the data on related 2,5-disubstituted tetrazoles [17].

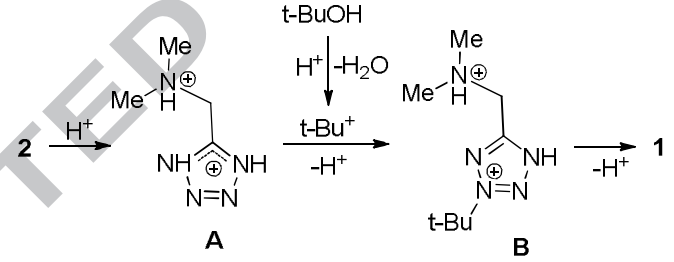

Scheme 2. Plausible mechanism of regioselective alkylation of **2**.

Tetrazole **1** belongs to 2,5-disubstituted tetrazoles, which show the weakest basicity of heteroring nitrogen atoms among neutral tetrazoles. Moreover, the presence of a substituent at the tetrazole ring C^5 atom obstructs the binding of metal cations with the most donor nitrogen atom N^4 by steric reason. Hence, successful complexation of 2,5-disubstituted tetrazoles needs the use of weakly coordinating solvents and sometimes the removal of competitive ligands like water [21]. Obviously, the presence of highly basic amino group in chelating position in relation to N^4 endocyclic atom in ligand **1** significantly enhances its complexing ability in comparison with 2,5-dialkyltetrazoles. We found that this ligand reacted with copper(II) chloride dihydrate in 1,2-dichloroethane to give complex $[Cu_2L_2Cl_4]$ (**3**) (Scheme 3). Its recrystallization from chloroform–toluene mixture generated crystals of solvated complex $[Cu_2L_2Cl_4]\cdot 2CHCl_3$ (**3*s***).

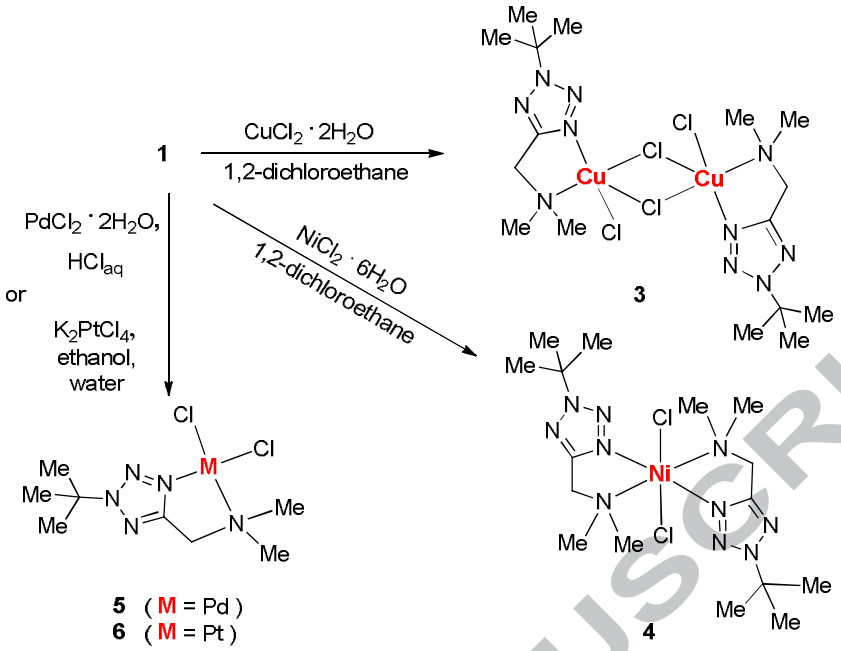

Scheme 3. Complexation of ligand **1**.

Nickel(II) chloride hexahydrate reacted with ligand **1** in 1,2-dichloroethane giving $[NiL_2Cl_2]$ (**4**). Complexes $[PdLCl_2]$ (**5**) and $[PtLCl_2]$ (**6**) were obtained by reaction of tetrazole **1** with palladium(II) chloride dihydrate in 1M HCl aqueous solution or with potassium tetrachloridoplatinate(II) in water/ethanol mixture, respectively.

Thermal analyses of the synthesized complexes were performed from room temperature to 500 °C to examine their thermal stability. Thermogravimetric (TG) and differential scanning calorimetry (DSC) curves of the compounds are presented in Figs. S1–S5. Thermal stability of complexes **3**, **4**, **5**, and **6** strongly depends upon the nature of the metal, increasing in the order Cu < Ni < Pd < Pt. The first stage of their thermolysis proceeds in the endothermic mode, with a peak located at 150, 190, 222 and 288 °C for complexes **3**, **4**, **5**, and **6**, respectively. Solvated complex **3*s*** loses solvate molecules above 90 °C (endothermic peak of this process is located at 107 °C) to give complex **3**. This conclusion follows from X-ray powder pattern of the sample obtained from complex **3*s*** by its thermal treatment at 100 °C, and also from the same thermal behavior of complexes **3** and **3*s*** above 120 °C (Figs. S1, S2).

3.2. Crystal structures description

Crystal structures of complexes **3**, **3*s***, and **4–6** were obtained from single crystal X-ray data collected at a temperature of 100 K. Crystal data, data collection, and structure refinement details for the compounds are gathered in Table 1. All they did not reveal phase transitions in the temperature range 100–296 K.

Table 1. Main crystal data and structure refinement details for complexes **3**, **3*s*** and **4**–**6**.

	Complex **3**	Complex **3*s***	Complex **4**	Complex **5**	Complex **6**
Formula	$C_{16}H_{34}Cl_4Cu_2N_{10}$	$C_{18}H_{36}Cl_{10}Cu_2N_{10}$	$C_{16}H_{34}Cl_2N_{10}Ni$	$C_8H_{17}Cl_2N_5Pd$	$C_8H_{17}Cl_2N_5Pt$
Formula weight	635.41	874.15	496.14	360.56	449.25
T (K)	100(2)	100(2)	100(2)	100(2)	100(2)
Crystal system	Triclinic	Monoclinic	Monoclinic	Orthorhombic	Orthorhombic
Space group	$P\bar{1}$	$P2_1/c$	$P2_1/n$	*Pbca*	*Pbca*
Crystal size (mm)	0.32×0.29×0.26	0.26×0.16×0.08	0.16×0.15×0.08	0.46×0.46×0.20	0.23×0.20×0.06
a (Å)	10.77560(10)	10.8243(3)	11.37100(10)	10.6319(5)	10.61560(10)
b (Å)	10.86180(10)	11.8529(3)	10.12770(10)	11.3462(6)	11.3826(2)
c (Å)	12.00230(10)	27.9693(7)	11.89850(10)	22.1501(11)	22.1138(3)
α (°)	87.0170(4)	90	90	90	90
β (°)	89.9926(5)	92.6177(15)	117.9931(5)	90	90
γ (°)	70.2578(4)	90	90	90	90
V (Å^3)	1320.19(2)	3584.70(16)	1209.94(2)	2672.0(2)	2672.08(6)
Z	2	4	2	8	8
D_c (g cm^{-3})	1.598	1.620	1.362	1.793	2.233
μ (mm^{-1})	2.041	1.960	1.046	1.771	10.885
Measured refls.	32776	33710	15160	21483	20864
Independent refls.	8735	8220	2391	2447	2472
R_{int}	0.0124	0.0271	0.0178	0.0155	0.0233
Restraints	0	0	43	0	0
Parameters	299	371	170	150	150
*R*1/*wR*2[$I>2\sigma(I)$]	0.0163/0.0450	0.0432/0.1138	0.0396/0.1064	0.0228/0.0722	0.0174/0.0446
*R*1/*wR*2 [all data]	0.0172/0.0455	0.0516/0.1176	0.0438/0.1102	0.0230/0.0723	0.0208/0.0459
Goodness-of-fit	0.997	1.051	1.017	1.079	1.006

*3.2.1. Complexes $[Cu_2L_2Cl_4]$ (**3**) and $[Cu_2L_2Cl_4]\cdot 2CHCl_3$ (**3*s***)*

Complex **3** and solvated complex **3*s*** include binuclear complex molecules of the composition $Cu_2L_2Cl_4$ (L is ligand **1**). The structures of complex molecules in **3** and **3*s*** were found to be similar and therefore the same atom-numbering scheme for them was used in the present work (Fig. 1). Whereas complex **3** is triclinic (the space group $P\bar{1}$), complex **3*s*** crystallizes in the monoclinic space group $P2_1/c$. In both compounds, there is one complex molecule in the asymmetric unit, including two independent ligands L. In complex **3*s***, the asymmetric unit contains additionally two chloroform molecules. All the atoms of the compounds occupy general positions.

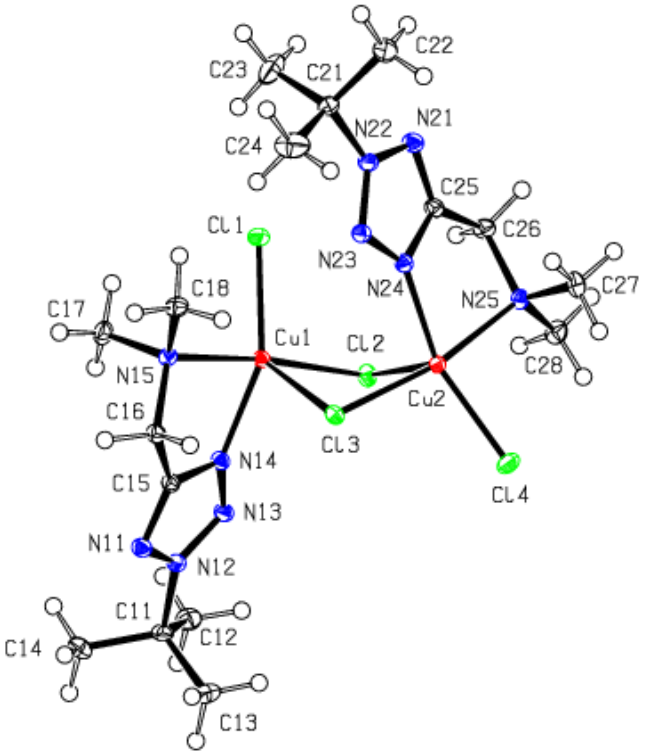

Fig. 1. Binuclear complex molecule in the crystal structure of **3**, with the atom-numbering scheme (the same atom-numbering is used for complex molecule of **3*s***). Displacement ellipsoids are drawn at the 50 % probability level. The hydrogen atoms are shown as spheres of arbitrary radii.

In complex molecules of **3** and **3**, the copper atoms Cu1 and Cu2 are linked together by double chlorine bridge at the expense of Cl2 and Cl3 atoms. Each copper atom is bonded to one ligand L through the tetrazole ring N^4 and the dimethylamino N atoms, so both independent ligands L show chelating mode with five-membered chelate rings.

Coordination environment of Cu1 and Cu2 atoms forms considerably distorted square pyramids, with τ-descriptors [22] for penta-coordination of 0.37 (Cu1) and 0.26 (Cu2) in complex **3**, and respectively 0.33 and 0.31 in complex **3*s*** (τ = 0 for an ideal square pyramid and τ = 1 for an ideal trigonal bipyramid). Whereas all basal bonds are usual in both compounds, the apical bonds Cu1–Cl3 and Cu2–Cl2 are significantly elongated and can be considered as semi-coordinated (Table 2). As a result of considerable distortion of the square pyramids, the mean deviation of the basal atoms from their least squares planes show rather large values of 0.3062(3) Å (Cu1) and 0.2448(3) Å (Cu2) in complex **3**, and respectively 0.3094(13) and 0.2480(13) Å in complex **3*s***. The dihedral angle between the basal planes of two pyramids is 14.856(17)° in **3** and 15.13(6)° in **3*s***.

Table 2. Coordination bond lengths (Å) and angles (°) in complexes **3** and **3*s***.

	Complex **3**	Complex **3*s***
Cu1 polyhedron		
Cu1–N14	2.0232(7)	2.004(3)
Cu1–N15	2.1013(7)	2.094(3)
Cu1–Cl1	2.2331(2)	2.2313(9)
Cu1–Cl2	2.2584(2)	2.2680(9)
Cu1–Cl3	2.7592(2)	2.8192(10)
N14–Cu1–N15	79.66(3)	79.69(12)
N14–Cu1–Cl1	150.10(2)	150.83(9)
N15–Cu1–Cl1	92.24(2)	92.77(9)
N14–Cu1–Cl2	95.95(2)	95.46(9)
N15–Cu1–Cl2	172.14(2)	170.83(9)
Cl1–Cu1–Cl2	94.731(8)	95.16(3)
N14–Cu1–Cl3	89.38(2)	88.22(10)
N15–Cu1–Cl3	86.13(2)	86.65(9)
Cl1–Cu1–Cl3	118.988(8)	119.68(3)
Cl2–Cu1–Cl3	87.316(7)	85.42(3)
Cu2 polyhedron		
Cu2–N24	2.0076(7)	1.993(3)
Cu2–N25	2.1006(7)	2.102(3)
Cu2–Cl4	2.2154(2)	2.2287(9)
Cu2–Cl3	2.2803(2)	2.2842(9)
Cu2–Cl2	2.7443(2)	2.6608(9)
N24–Cu2–N25	79.49(3)	79.49(11)
N24–Cu2–Cl4	153.69(2)	151.86(9)
N25–Cu2–Cl4	93.88(2)	93.46(8)
N24–Cu2–Cl3	90.35(2)	91.16(9)
N25–Cu2–Cl3	169.01(2)	170.25(8)
Cl4–Cu2–Cl3	97.098(8)	96.11(3)
N24–Cu2–Cl2	99.74(2)	100.09(8)
N25–Cu2–Cl2	90.35(2)	90.02(8)
Cl4–Cu2–Cl2	105.773(8)	107.17(3)
Cl3–Cu2–Cl2	87.249(7)	88.93(3)
Cu–Cl–Cu bridges		
Cu1–Cl2–Cu2	86.118(7)	87.17(3)
Cu1–Cl3–Cu2	85.347(7)	83.15(3)
Cu1···Cu2	3.434(3)	3.4100(5)

The tetrazole rings show the feature, observed often enough in complexes of 2- and 2,5-substituted tetrazoles, namely formally single bonds N^2–N^3 are shorter that formally double bonds N^3–N^4. In two rings N11–C15 and N21–C25, the lengths of these bonds are N^2–N^3 = 1.3162(9)/1.3118(10), N^3–N^4 = 1.3254(9)/1.3231(10) Å in complex **3**, and N^2–N^3 = 1.303(4)/1.314(4), N^3–N^4 = 1.325(4)/1.322(4) Å in **3*s***.

Both complexes reveal non-classic intramolecular hydrogen bonds C16–H16A···Cl3 [hydrogen bond geometry in **3/3*s***: D···A = 3.3026(8)/3.329(4) Å, D–H···A = 120/121°] (Fig. 2).

In complex **3*s***, there are additional non-classic hydrogen bonds of chloroform H atoms, binding chloroform molecules with complex molecules. These are bifurcate bonds C1–H1···Cl3 [D···A = 3.552(4) Å, D–H···A = 143°] and C1–H1···Cl4 [D···A = 3.525(5) Å, D–H···A = 140°] of one chloroform molecule, and the bonds C2–H2···Cl4[a] of another molecule [D···A = 3.518(4) Å, D–H···A = 145°; symmetry code: (a) 1–*x*, 1–*y*, 1–*z*].

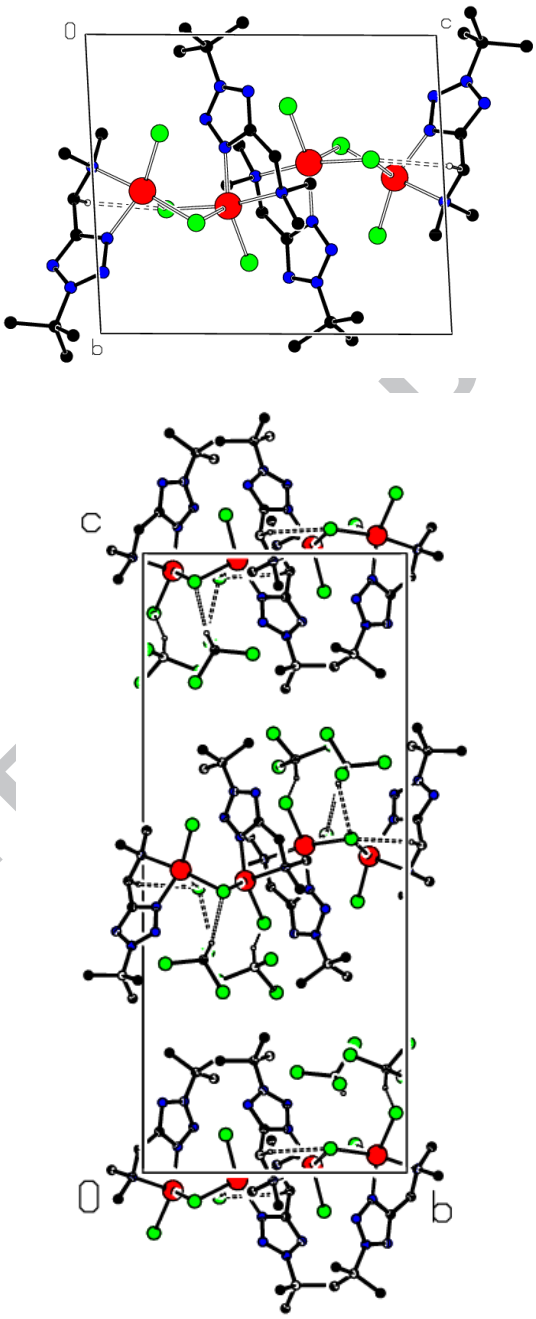

Fig. 2. Crystal packing of complexes **3** (top) and **3*s*** (bottom), viewed along the *a* axis. Dashed lines show hydrogen bonds. Only the hydrogen atoms participating in hydrogen bonds are shown.

Although complexes **3** and **3*s*** crystallize in different space groups and have different unit cell dimensions, nevertheless similar features in their crystal packing are observed. In both compounds, we can select "layers" of complex molecules, parallel to the *ac* plane in complex **3** and the *ab* plane in complex **3*s***. A side view of such "layers" is provided by Fig. 2. It is clearly seen that the arrangement of complex molecules in the "layers" is rather similar in both compounds. As a result, the unit cell dimensions *a* and *c* of **3** are close to respectively *a* and *b* of **3*s***. In solvated complex, chloroform molecules are located on both sides of each "layer" and are hydrogen-bonded to its complex molecules. These structural features allow to explain easy transformation of complex **3s** to complex **3** at about 100 °C.

*3.2.2. Complex [NiL_2Cl_2] (**4**)*

Complex **4** crystallizes in the monoclinic space group $P2_1/n$, with two formula units in the unit cell. The compound presents a mononuclear complex, in which the nickel atom lies on the inversion centre. In crystals of **4**, ligand molecule L is disordered over two positions, with site occupancy factors 0.9044(19) (site *A*) and 0.0956(19) (site *B*). Fig. 3*a* shows the complex molecule, in which ligand L occupies site *A*, whereas Fig.3*b* illustrates both sites together. It should be noted that there is one non-disordered atom in ligand L, *viz* the dimethylamino nitrogen atom N5.

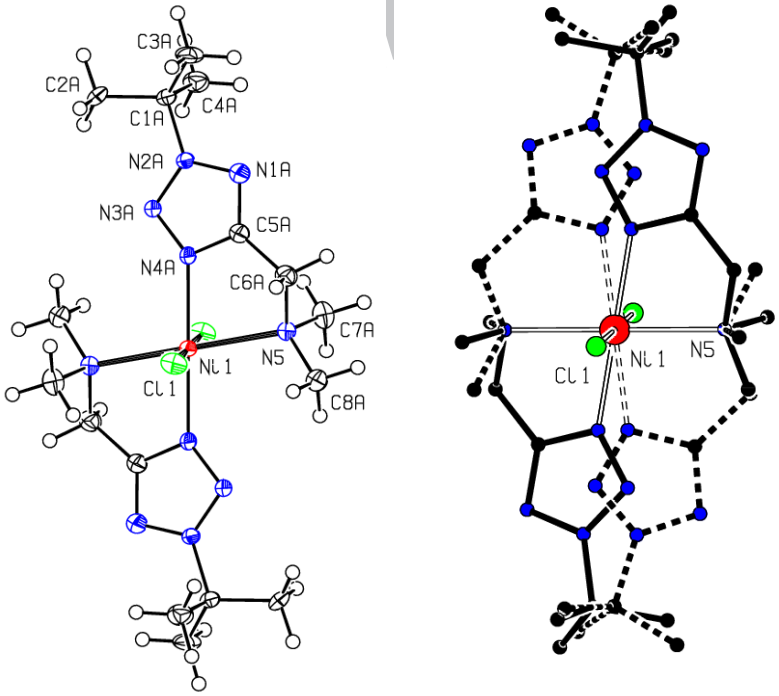

(*a*) (*b*)

Fig. 3. (a) Complex molecule of **4** with ligand L being in high-occupancy site *A* [the atom-numbering is given for the asymmetric unit; unlabeled atoms are related to the labeled ones by the symmetry operation: 1–*x*, 1–*y*, –*z*; displacement ellipsoids are drawn at the 50% probability level; the hydrogen atoms are shown as spheres of arbitrary radii]. (b) Comparison of sites *A* (the bonds are shown as solid lines) and *B* (the bonds are shown as dashed lines) of disordered ligand L in complex **4** [the hydrogen atoms are omitted for clarity].

Further, structural description of complex **4** is given only for high-occupancy site *A* of ligand L (the atom-numbering of L includes "A").

The nickel atom is surrounded by two chlorine atoms and two ligands L, coordinated in chelate mode *via* the tetrazole ring N^4 and the dimethylamino nitrogen atoms to form a five-membered chelate ring. Two chlorine and four nitrogen atoms form around the nickel atom a distorted octahedron, with chlorine atoms in the axial positions. Whereas Ni–Cl bonds are elongated, all equatorial Ni–N bonds show usual lengths, namely Ni1–Cl1 = 2.4302(6), Ni1–N4A = 2.062(2), and Ni1–N5 = 2.241(2) Å. Among the valence angles around the nickel atom, the chelate angle N4A–Ni1–N5 of 78.94(8)° is the smallest angle. All other coordination angles are in the range of 87.42(5)–101.06(8)° or equal to 180°.

There are no hydrogen bonds in the crystal structure of complex **4**. Its crystal packing, shown in Fig. 4, is stabilized only by van der Waals interactions.

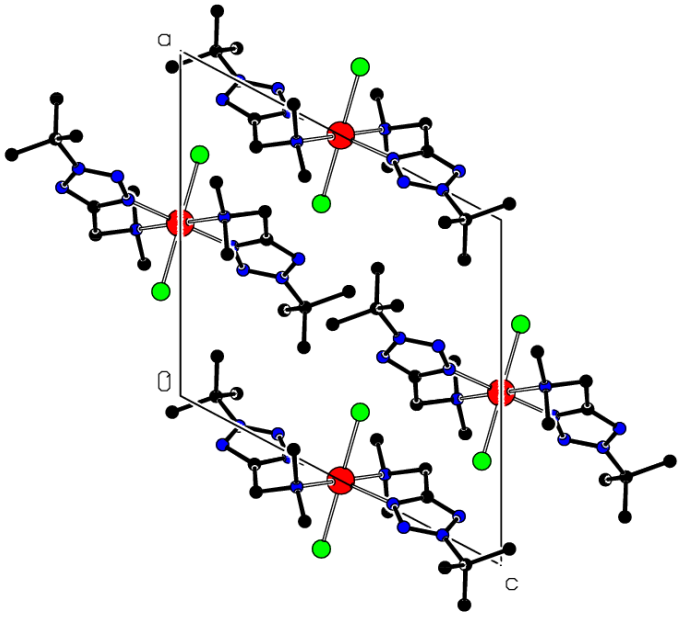

Fig. 4. Crystal packing of **4**, viewed along the *b* axis. Hydrogen atoms are omitted for clarity.

*3.2.3. Complexes [PdLCl$_2$] (**5**) and [PtLCl$_2$] (**6**)*

Complexes **5** and **6** were found to be isomorphous, crystallizing in the orthorhombic space group *Pbca* with eight formula units in the unit cell. The same asymmetric unit and the same atom-numbering schemes were used here for these two compounds. They present mononuclear complexes, whose molecular structure is illustrated in Fig. 5 for chloride complex **5** as an example.

The metal atoms are surrounded by two chlorine atoms and one ligand molecule L, coordinated in a chelate mode through the tetrazole ring N4 and the dimethylamino N5 nitrogen atoms. The chlorine and nitrogen atoms form around the metal atoms distorted coordination squares. Coordination characteristics of **5** and **6** are given in Table 3.

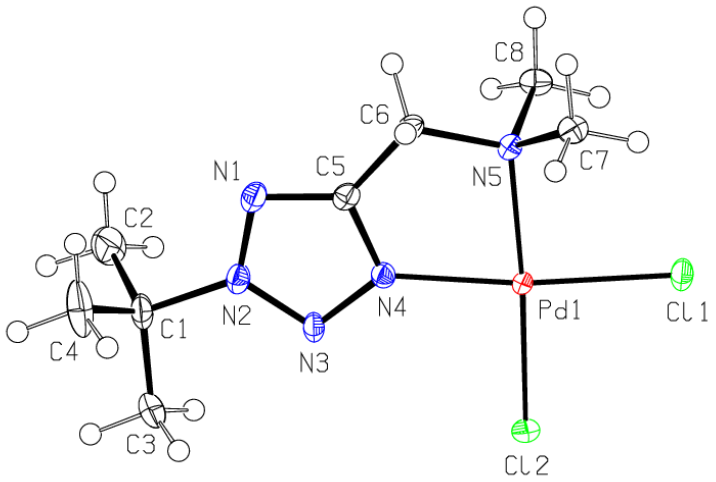

Fig. 5. Molecular structure of complex **5**, with the atom-numbering scheme. Displacement ellipsoids are drawn at the 50% probability level. The hydrogen atoms are shown as spheres of arbitrary radii.

Table 3. Coordination bond lengths (Å) and angles (°) in complexes **5** and **6**.

	Pd(II) complex **5**	Pt(II) complex **6**
(Pd1/Pt1)–N4	1.992(3)	1.967(3)
(Pd1/Pt1)–N5	2.097(3)	2.084(3)
(Pd1/Pt1)–Cl1	2.2809(9)	2.2845(10)
(Pd1/Pt1)–Cl2	2.3007(8)	2.3037(8)
N4–(Pd1/Pt1)–N5	81.96(10)	81.63(11)
N4–(Pd1/Pt1)–Cl1	173.43(8)	173.56(9)
N5–(Pd1/Pt1)–Cl1	92.47(7)	92.74(7)
N4–(Pd1/Pt1)–Cl2	94.27(8)	95.06(9)
N5–(Pd1/Pt1)–Cl2	175.56(7)	176.27(7)
Cl1–(Pd1/Pt1)–Cl2	91.15(3)	90.48(3)

As can be seen from Table 3, all coordination bonds (Pd/Pt)–Cl and (Pd/Pt)–N are usual. Coordination cores (Pd/Pt)N_2Cl_2 are substantially planar, with mean deviations of their atoms from corresponding least-squares planes of 0.0244(12) Å in complexes **5** and 0.0217(12) Å in complex **6**. The valence angles N4–(Pd1/Pt1)–N5 are close to those in complexes **3**, **3*s*** and **4,** being lower than 90° as a result of their including in five-membered chelate cycles.

In the crystal structures of **5** and **6**, there are only non-classic intermolecular hydrogen bonds

C6–H6A···Cl2^{b} between the methylene H and Cl atoms of neighboring complex molecules [hydrogen bond geometry (Pd/Pt): D···A = 3.487(3)/3.504(4)°, D–H···A = 149/151°] (symmetry code (b) as in Fig. 6). These bonds are responsible for formation of centrosymmetric dimers, shown in Fig. 6.

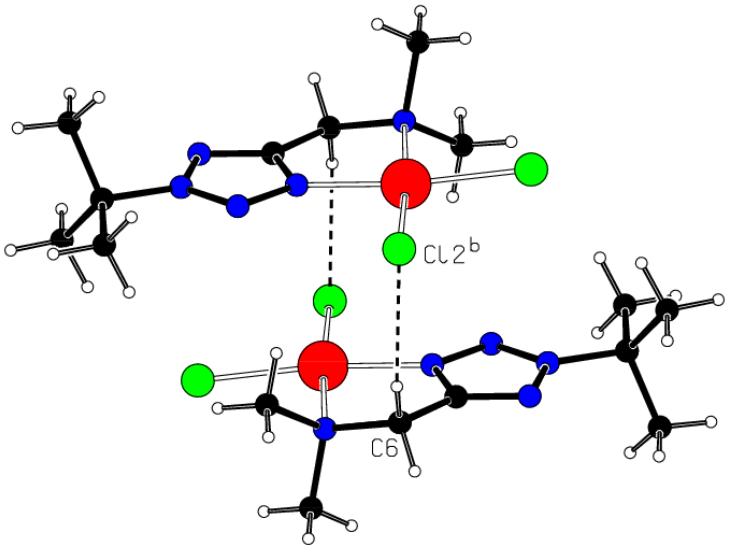

Fig. 6. Hydrogen-bonded centrosymmetric dimer in the crystal structure of **5**. Symmetry code (b): 1–*x*, 1–*y*, 1–*z*.

*3.3 Magnetic properties of complex **3***

The presence of separated Cu_2Cl_4 units in complex **3** determines the interest in the magnetic investigation of the compound. Its magnetic properties were investigated by temperature-dependent magnetic susceptibility measurements in the temperature range between 2 and 300 K. Fig. 7 shows the experimental data and the theoretical fit in the form of μ_{eff} *vs*. *T*. The effective magnetic moment μ_{eff} is of 2.56 μ_B at 300 K, and remains nearly constant with decreasing temperature down to 70 K. Upon further lowering the temperature, μ_{eff} rapidly decreases to 2.09 μ_B at 5 K. The μ_{eff} values in the temperature range 300–70 K are in a good agreement with a theoretical value of 2.63 μ_B for two copper(II) ions with *g*-factor of 2.15. The decreasing of the μ_{eff} below 70 K indicates the presence of weak antiferromagnetic exchange interactions between spins of the copper(II) cations. The model of exchange-coupled dimer (spin Hamiltonian $H = -2JS_1S_2$) was used for the analysis of the experimental μ_{eff}(T) dependence. The best fit was reached with *g*-factor of 2.08 and exchange interaction parameter *J* of –2.0 cm^{-1}.

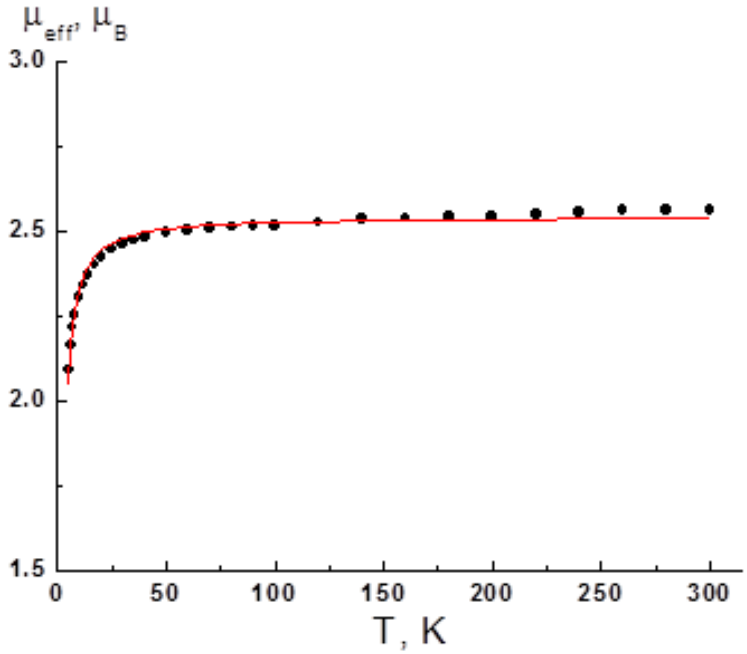

Fig. 7. Temperature dependence of μ_{eff} for compound **3** (•) per dinuclear unit. The red solid line represents the best theoretical fit.

Several attempts have been made to establish the correlations between structural and magnetic properties of binuclear copper(II) complexes with Cu(μ-Cl)$_2$Cu core [23–26]. It has been shown that exchange coupling constant J is determined by such structural parameters as coordination geometry of copper atoms, the bridging angles Cu–Cl–Cu, and the Cu···Cu distances. In complexes with square-pyramidal coordination of two copper atoms, magneto-structural correlations were found to depend on the relative orientation of square pyramids.

Compound **3**, investigated in the present work, belongs to the group of complexes, in which copper(II) square pyramids share a base-to-apex edge and their basal planes are approximately parallel. In such complexes, super exchange pathway between the metal centres will take place mainly through a π* type interaction between the $d_{x^2-y^2}$ orbitals of Cu^{2+} ions and the p-orbitals of chlorine bridging ligand as shown using extended Hückel calculations [24]. For an ideal geometry with a square core, the overlap integral between the former orbitals would be zero. However, due to deviations of Cu(μ-Cl)$_2$Cu core from the ideal square, these complexes usually show antiferromagnetic or ferromagnetic coupling with relatively small coupling constants ($-10 < J < +10$ cm^{-1}) [25]. A strong correlation has been found between J value and the φ/R ratio, where φ is the Cu–Cl–Cu bridging angle and R is the longest Cu–Cl distance in the chloride bridge [26]. It was estimated that the exchange interaction is ferromagnetic if φ/R ratio lies within the range 31–34.5 deg·Å^{-1}, otherwise it is antiferromagnetic. In the case of complex **3**, where the copper(II) centres Cu1 and Cu2 are not identical, two φ/R values can be calculated,

namely φ/R = 30.9 deg·Å^{-1} [for R(Cu1–Cl3), φ(Cu1–Cl3–Cu2)] and φ/R = 31.4 deg·Å^{-1} [for R(Cu2–Cl2), φ(Cu2–Cl2–Cu1)]. Both calculated values of φ/R are very close to the lower limit of 31 deg·Å^{-1} of the above interval. Because the correlation $J(\varphi/R)$ presents only an approximation, both positive and negative small coupling constants J should be expected for complex **3** from this correlation. Therefore, small experimental value J of –2.0 cm^{-1}, obtained for complex **3**, does not contradict the above empirical magneto-structural correlation.

*3.4. Antiproliferative activity of complex **6***

In the last decade, various tetrazole-containing platinum(II) and platinum(IV) complexes attracted a great deal of attention as promising antitumor agents [11, 27–32]. Due to variety of possible substitutes and the ability of the tetrazole ring to decrease toxicity of modifying medicines, tetrazole-based ligands have been utilized to design new generation of perspective platinum(II) complexes with lower toxicity [30, 31], increased water solubility [31, 32], and the ability to overcome tumor resistance to the common platinum drugs [28–31].

In our previous works, we have been focused on antiproliferative activity of platinum(II) complexes with N-substituted tetrazoles as carrier ligands. In a good agreement with classic SAR rules, cytotoxicity of such complexes turned out to be dependent on their geometry and lipophilicity. The most active species *cis*-Pt(5-amino-2-*tert*-butyltetrazole)$_2$Cl$_2$ appeared to be at least as active as cisplatin in a number of cisplatin-sensitive cancer cell lines and also able to overcome cross-resistance in cisplatin-resistant cell lines [31]. However, *cis*-isomeric platinum complexes with *N*-substituted tetrazoles were found to be prone to thermal isomerization both in the solid state and in the solution. Therefore, we were interested in designing structurally related complexes with fixed *cis* geometry of the platinum(II) coordination center.

To this aim, complex **6** was obtained and its antiproliferative activity was investigated in human cervical carcinoma cell line (HeLa) using trypan-blue exclusion assay. Cisplatin and carboplatin were included into the assay as a positive control. The determined IC_{50} values are summarized in Figure S6. Tetrazole complex **6** demonstrates promising activity, with IC_{50} value of 3.9 μM being average between those of cisplatin (0.6 μM) and carboplatin (12.5 μM). Free ligand is inactive, with IC_{50} exceeding 100 μM. It should be noted that complex **6** demonstrated lower activity in comparison with parent *cis*-Pt(5-amino-2-*tert*-butyltetrazole)$_2$Cl$_2$, which showed IC_{50} of 0.9 μM in HeLa cell line [31], but appeared to be more active than corresponding *trans*-isomeric complex *trans*-Pt(5-amino-2-*tert*-butyltetrazole)$_2$Cl$_2$ with IC_{50} of 5.6 μM in HeLa cell line [11].

4. Conclusion

Novel tetrazole derived Mannich base, namely 5-(*N*,*N*-dimethylaminomethyl)-2-*tert*-butyltetrazole, was synthesized and used as ligand to obtain coordination compounds with Cu(II), Ni(II), Pd(II), and Pt(II) chlorides. As was expected, tetrazole ligands in all the complexes are coordinated by metals in chelate fashion *via* N^4 atom of the tetrazole heteroring and N atom of the dimethylamino group. However, the composition of the complexes, coordination environment of metals and their coordination polyhedra were found to be different, depending on the nature of the metal. All the complexes have molecular structure. Thermal stability of the synthesized complexes increases in the following order: Cu < Ni < Pd < Pt. Platinum(II) chloride complex was found to have promising antiproliferative activity against human cervical carcinoma cells, with IC_{50} value being average between those of cisplatin and carboplatin. Binuclear copper(II) complex shows weak antiferromagnetic coupling between metal cations.

Acknowledgements

This work was supported by Belarusian Republican Foundation for Fundamental Research (grant X16P-009).

Appendix A. Supplementary material

CCDC deposition numbers: 1831886, 1831887, 1831888, 1831889, and 1831890 contain the supplementary crystallographic data for complexes **3**, **3*s***, **4**, **5** and **6**, respectively. These data can be obtained free of charge *via* http://www.ccdc.cam.ac.uk/conts/retrieving.html, or from the Cambridge Crystallographic Data Centre, 12 Union Road, Cambridge CB2 1EZ, UK; fax: (+44) 1223-336-033; or e-mail: deposit@ccdc.cam.ac.uk.

References

[1] S. Bala, N. Sharma, A. Kajal, S. Kamboj, V. Saini, Int. J. Med. Chem. 2014 (2014) 191072.

[2] S.G. Subramaniapillai, J. Chem. Sci. 125 (2013) 467.

[3] V.P. Karavai, P.N. Gaponik, Chem. Heterocycl. Compd. 27 (1991) 55.

[4] A.R. Katritzky, B.E.-D.M. El-Gendy, B. Draghici, C.D. Hall, P.J. Steel, J. Org. Chem. 75 (2010) 6468.

[5] D.O. Ivashkevich, A.S. Lyakhov, S.V. Voitekhovich, P.N. Gaponik, Acta Crystallogr., Sect. C 58 (2002) m563.

[6] A.S. Lyakhov, S.V. Voitekhovich, L.S. Ivashkevich, P.N. Gaponik, Acta Crystallogr., Sect. C 66 (2010) m22.

[7] M.C. Burla, R. Caliro, B. Carrozzini, G.L. Cascarano, C. Cuocci, C. Giacovazzo, V. Mallamo, A. Mazzone, G. Polidori, J. Appl. Crystallogr. 48 (2015) 306.

[8] G. M. Sheldrick, Acta Crystallogr., Sect. C: Struct. Chem. 71 (2015) 3.

[9] L. J. Farrugia, J. Appl. Cryst. 30 (1997) 565.

[10] A. L. Spek, Acta Crystallogr., Sect. D: Biol. Crystallogr. 65 (2009) 148.

[11] S.V. Voitekhovich, T.V. Serebryanskaya, A.S. Lyakhov, P.N. Gaponik, O.A. Ivashkevich, Polyhedron 28 (2009) 3614.

[12] Yu.P. Istomin, E.A. Zhavrid, E.N. Alexandrova, O.P. Sergeyeva, S.V. Petrovich, Exp. Oncol. 30 (2008) 5.

[13] A.O. Koren, P.N. Gaponik, Chem. Heterocycl. Compd. 26 (1990) 1366.

[14] J.V. Filippova, A.G. Sukhanova, S.V. Voitekhovich, V.E. Matulis, G.T. Sukhanov, Y.V. Grigoriev, O.A. Ivashkevich, J. Het. Chem. 45 (2012) 965.

[15] S.V. Voitekhovich, A.S. Lyakhov, L.S. Ivashkevich, P.N. Gaponik, Tetrahedron Lett. 53 (2012) 6111.

[16] S.V. Voitekhovich, A.S. Lyakhov, L.S. Ivashkevich, V.E. Matulis, Y.V. Grigoriev, P.N. Gaponik, O.A. Ivashkevich, Tetrahedron 68 (2012) 4962.

[17] A.D. Lisakova, D.S. Ryabukhin, R.E.Trifonov, V.A.Ostrovskii, A. V.Vasilyev, Tetrahedron Lett. 56 (2015) 7020.

[18] A.P. Mosalkova, S.V. Voitekhovich, A.S. Lyakhov, L.S. Ivashkevich, J. Lach, B. Kersting, P.N. Gaponik, O.A. Ivashkevich, Dalton Trans. 42 (2013) 2985.

[19] A.O. Koren, P.N. Gaponik, V.A. Ostrovskii, Int. J. Chem. Kinet. 25 (1993) 1043.

[20] A.O. Koren, P.N. Gaponik, V.A. Ostrovskii, Int. J. Chem. Kinet. 27 (1995) 919.

[21] P.N. Gaponik, S.V. Voitekhovich, O.A. Ivashkevich, Russ. Chem. Rev. 75 (2006) 507.

[22] A. W. Addison, T. N. Rao, J. Reedijk, J. van Rijn, G. C. Verschoor, J. Chem. Soc., Dalton Trans. (1984) 1349.

[23] P. Torres-García, F. Luna-Giles, B. Garcia, C. Platas-Iglesias, D. Esteban-Gómez, E. Vinuelas-Zahinos, New J. Chem. 41 (2017) 8818; K. Skorda,T.C. Stamatatos, A.P.Vafiadis, A.T. Lithoxoidou, A.Terzis, S.P. Perlepes, J. Mrozinski, C.P. Raptopoulou, J.C. Plakatouras, E.G. Bakalbassis, Inorg. Chim. Acta 358 (2005) 565; H. Grove, J. Sletten, M. Julve, F. Lloret, J. Chem. Soc., Dalton Trans. (2001) 2487; M.T. Garland, J.-Y. Saillard, E. Spodine J. Crystallogr. Spectrosc. Res. 22 (1992) 467; W. E. Marsh, W. E. Hatfield, D. J. Hodgson, Inorg. Chem. 21 (1982) 2679.

[24] M. Rodriguez, A. Llobet, M. Corbella, Polyhedron 19 (2000) 2483.

[24] A. Rodríguez-Fortea, P. Alemany, S. Alvarez, E. Ruiz, Inorg. Chem. 41 (2002) 3769.

[26] W. E. Marsh, K. C. Patel, W. E. Hatfield, D. J. Hodgson, Inorg. Chem. 22 (1983) 511.

[27] S. Perfahl, A. Bodtke, J. Pracharova, J. Kasparkova, V. Brabec, J. Cuadrado, S. Stürup, C. Schulzke, P. J. Bednarski, Inorg. Chim. Acta 456 (2017) 86.

[28] S. Komeda, Y.-L. Lin, M.A. Chikuma, ChemMedChem 6 (2011) 987.

[29] S. Komeda, H. Takayama, T. Suzuki, A. Odani, T. Yamori, M. Chikuma, Metallomics 5 (2013) 461.

[30] M. Uemura, Y. Yoshikawa, K. Yoshikawa, T. Sato, Y. Mino, M. Chikuma, S. Komeda, J. Inorg. Biochem. 127 (2013) 169.

[31] T.V. Serebryanskaya, T. Yung, A.A. Bogdanov, A. Shchebet, S.A. Johnsen, A.S. Lyakhov, L.S. Ivashkevich, Zh.A. Ibrahimava, T.S. Garbuzenco, T.S. Kolesnikova, N.I. Melnova, P.N. Gaponik, O.A. Ivashkevich, J. Inorg. Biochem. 120 (2013) 44.

[32] E.A. Popova, T.V. Serebryanskaya, S.I. Selivanov, M. Haukka, T.L. Panikorovsky, V.V. Gurzhiy, I. Ott, R.E. Trifonov, V.Yu. Kukushkin, Eur. J. Inorg. Chem. 28 (2016) 4659.

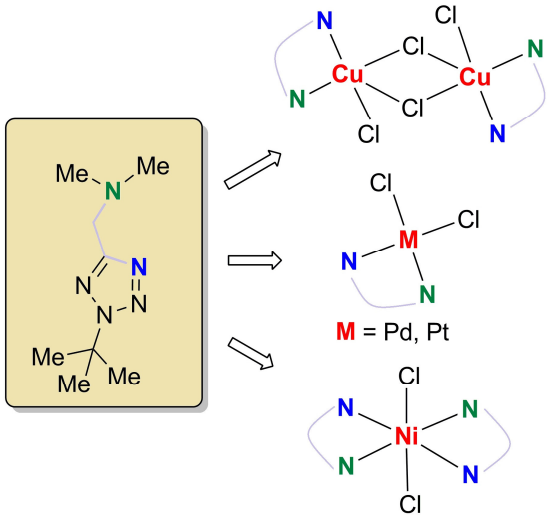

Synopsis

Novel tetrazole derived Mannich base is coordinated with transition metal chlorides in chelate fashion. The composition of the complexes and coordination geometry of the metals are different, depending on the nature of the metal. $[PtLCl_2]$ have promising antiproliferative activity against human cervical carcinoma cells. In $[Cu_2L_2Cl_4]$ copper(II) ions are weakly antiferromagnetically coupled.